An inkjet-printable fluorescent thermal sensor based on CdSe/ZnS quantum dots immobilised in a silicone matrix

L. Birchall [a], A. Foerster [a,*], G.A. Rance [b], A. Terry [c], R.D. Wildman [a], C.J. Tuck [a]

[a] *Centre for Additive Manufacturing, University of Nottingham, Nottingham NG8 1BB, United Kingdom*
[b] *Nanoscale and Microscale Research Centre, University of Nottingham, Nottingham NG7 2RD, United Kingdom*
[c] *AWE, Aldermaston, Reading RG7 4PR, United Kingdom*

A B S T R A C T

The drive towards device miniaturisation in fields such as microfluidics or microelectronics has established a need for non-intrusive, in situ temperature sensing, which is difficult to implement and manufacture in devices. Inkjet printing is a non-contact, maskless deposition method which is compatible with a wide range of materials and may enable the economical design and production of such devices. However, current inkjet-printed thermal sensors are predominantly based on resistance across printed circuits and do not meet the requirements for miniaturised devices. In this paper, an inkjet-printable material for luminescence-based temperature sensing is presented. Two-part reactive inks are developed using CdSe/ZnS quantum dots immobilised in an addition cure silicone matrix. Further platinum catalyst is added to resolve issues with catalyst poisoning by labile QD ligands, with the effect of catalyst loading on the degree of conversion and QD emission probed using Raman microscopy and well-plate reading, respectively. A mechanism for platinum-induced quenching is proposed. The inkjet printing of a bulk QD-silicone composite is successfully demonstrated for the first time, enabling a new route for devices with embedded luminescence thermometry. Confocal laser scanning microscopy is used to characterise the temperature response of the material, demonstrating sensing with a thermal coefficient of emission intensity of -0.68 to -0.93 % $°C^{-1}$ between 30 and 60 °C. We anticipate that this material has application for in situ thermal analysis and calibration within the fields of microfluidics.

1. Introduction

The drive towards device miniaturisation in electronics, optronics, and chemical and bio-analysis [1,2] raises a corresponding need for non-invasive, in situ thermal sensing for accurate calibration and analysis during device operation. For instance, within the fields of microfluidics and organ-on-a-chip, integrated sensors eliminate the need for manual sample collection, which is time-consuming, requires large working volumes, and can disturb the system [3]. However, direct sensor integration is challenging via conventional manufacturing: device fabrication is greatly complicated by multi-step processes, heat treatments, and material compatibility. Inkjet printing (IJP) is a non-contact deposition method which is suitable for biological applications as it prevents cross-contamination from the surface being printed on. Inkjet printing can produce electrodes and sensors on a range of substrates at low temperatures and has become an attractive manufacturing process for end-use products (including electronics [4,5],

chemisensors, [6] and microfluidics [7]) due to its capacity for multi-material deposition and the geometric freedom inherent to additive manufacturing techniques [8,9]. The drive for IJP of microfluidics has been broadly discussed by Waheed et al. [7]; moreover, it delivers small droplets (typically 20–50 μm) [10] and enables drop-on-demand material deposition compatible with microdevices with temperature sensitive substrates. It has been shown that inkjet printing is a viable technique for integrating various sensors to assess the metabolic activity of cells, one of the major challenges in maximising the potential of Organ-On-Chip systems. Moya et al. proposed an approach that integrates multiple sensors into the very thin, porous, sensitive membrane of a liver-on-chip device. Three electrochemical dissolved oxygen (DO) sensors were printed via inkjet along the microfluidic channel, enabling local online monitoring of oxygen concentration [3]. Printed DO sensors showed a linear response over a wide range of oxygen concentrations and showed very good performance with low detection limits.

Current inkjet-printable temperature sensors are well-suited for

wearable sensors; however, although IJP is capable of material deposition with 20–50 μm resolution [10], these sensors are typically on the order of cm [2] in size and sensing areas tens of mm [2], which limits spatial resolution and capacity for planar or 3D imaging. [11,12] The vast majority of IJP temperature sensors reported are resistance temperature detectors (RTDs) or thermistors, both of which measure electrical resistance as a function of temperature. Resistance-based sensing materials for inkjet typically require post-processing heat treatments at around 150 °C and include silver [13–17], nickel oxide [18], carbon nanomaterials [19–21], and PEDOT:PSS polymers [19–21]. However, while RTDs have the advantages of being easy to manufacture, sensitive, and stable, RTDs are not suitable for measurement of sub-millimetre areas or transient temperatures due to their large sensing areas. They are also active devices with milliamp scale power, which may alter measurement due to heat generation. The thermal coefficient of resistance of inkjet-printed materials is currently limited to 0.1–0.3 % C^{-1}, the one exception being the thermistor-like sensor reported by Trudeau et al. which has six degrees of magnitude change in resistance but its 17–36 °C sensing range is below body temperature [17]. In summary, IJP resistance-based thermal sensors have limited spatial resolution and do not achieve the sub-degree thermal resolution in the physiological range, which is a barrier to their use in microdevices and in cell culture and biomedical applications.

Luminescence thermometry – temperature measurement based on changes in the fluorescence of a material – can address requirements for integrated sensing in microdevices [22,23]. This approach has high spatial and thermal resolution, which makes it suitable for in situ detection of localised "hot-spots" in microdevices and for the monitoring of complex systems. The spatial resolution of fluorescence-based sensing is determined by size of the emissive species and the data collection method [22]; microscale resolution is typical, using embedded optical fibres or waveguides for remote sensing and fluoresecence microscopy for planar or 3D sensing. The set up for fluorescence-based measurements is more complex than that of IR thermography, requiring an excitation source and optical set up, and the method can introduce large systematic uncertainties as fluorescent parameters are compared to a reference image taken at room temperature, in addition to sensitivity to lighting conditions. However, the difference in emissivity between device materials and solvents can reduce the accuracy of IR measurements; furthermore, the technique uses wavelengths between 0.7 and 20 μm, while the solvents of biochemical reactions show strong absorption > 1 μm, which limits its application for microfluidics. The spatial resolution achievable using IR is also diffraction-limited; fluorescence-based measurements using standard fluorescence microscopes have resolutions down to 1 μm, while IR thermography examples in microfluidics literature are between 3 and 10 μm [24]. Choudhury et al. demonstrated sensing with 3.6 μm axial and 0.6 μm lateral resolutions within a microchannel using confocal laser scanning microscopy with a waveguide [25]. Overall, fluorescence sensors may be desired in applications where high spatial and thermal resolution are required, such as microfluidics involving PCR and microreactors. An inkjet-printable luminescence-based sensing material could enable the production of devices with integrated sensing geometries that are challenging or impossible to achieve by conventional means.

Quantum dots (QDs) are fluorescent semiconductor nanoparticles with outstanding emission properties for luminescence thermometry, specifically high photostability, high quantum yields, small diameter, and a narrow, tuneable emission peak [26,27]. High-resolution temperature sensing with QDs has been demonstrated using intensity [28–32], spectral [25,33–36], and/or lifetime [37] based measurement of fluorescence. As temperature increases, QD fluorescence undergoes characteristic changes: emission intensity decreases, the emission peak red-shifts and broadens, and the luminescence lifetime decreases [38, 39]. Overall, QDs are excellent temperature nanoprobes: the spectral and lifetime thermal coefficients of QDs are high [37,40] and emission intensity decreases linearly with temperature in the reversible region,

resulting in a constant thermal sensitivity and simple calibration.

Quantum dots require a carrier medium to be processable by inkjet printing [10]. While QD-containing jetting inks are commonly formulated using solvents alone [41–44, immobilisation of QDs in polymer matrices can improve QD dispersion and reduce quenching to improve the photoluminescent efficiency [45,46]. Immobilisation of emitters may further prevent changes in the fluorophores that are known to lead to reduced thermal accuracy in semi-invasive sensing, including changes in concentration, absorption on microchannel walls, and thermophoresis. [24] Silicone is an ideal polymer matrix for optical sensing applications due to its high optical transparency, refractive index, and thermal stability [47]; bulk QD-silicone nanocomposites have been investigated for use as conversion films for LEDs [48–54]. Additionally, polydimethylsiloxane (PDMS) is the most commonly used elastomer in the production of microfluidic devices and is suitable for a range of biomedical applications [55]. As silicones are thermoset polymers which cross-link through various mechanisms [47,56,57], reactive IJP is a feasible route to elastomers from low viscosity inks [58–62].

As typical commercial silicones for both LED encapsulants and microfluidic devices are addition cure, advantageous for their minimal by-products and shrinkage, [47,57] this mechanism has been explored in this work. However, hydrosilylation of addition cure silicones is hindered by QDs [63–65]. Labile stabilising ligands on the quantum dot surface – notably primary amines in CdSe-based QDs [66,67] – detach and poison the platinum catalyst. This prevents ambient cross-linking and therefore complicates device fabrication in terms of heat treatments and compatibility with potential materials or components.

In this paper, increased platinum catalyst loadings are explored as a strategy to enable reactive inkjet printing of QD-silicone composites for integrated thermal sensing. The effects of platinum concentration on silicone curing and on QD fluorescence are investigated and suggested mechanisms are given. The temperature-dependent fluorescence of the material is assessed using well-plate reading and confocal microscopy, confirming that linear thermal coefficients are observed for both emission- and spectral-based luminescence sensing. Inkjet printing of a QD-silicone composite is demonstrated for the first time, enabling printed devices with integrated microscale sensing areas for luminescence thermometry, such as for monitoring inside microfluidic channels or for detection of hot-spots within microdevices.

2. Experimental

2.1. Materials

Inks were prepared from PlatSil® SiliGlass (Polytek), octyl acetate ≥ 99 % and platinum (II) chloride 98 % (both Sigma Aldrich). CdSe/ZnS core-shell quantum dots (Ocean Nanotech, λ_{max} 630 nm, Fig. S1) were supplied in powder form with octadecylamine stabilising ligands. Glass slides were coated in 1 H,1 H,2 H,2 H-perfluorooctyl-trichlorosilane 97 % (Sigma Aldrich) to prepare sufficiently hydrophobic substrates for printing [59]. All chemicals were used as received without further treatment.

2.2. Ink preparation

Ink A and Ink B addition cure inks were prepared from SiliGlass with 50 wt% octyl acetate solvent, formulated to have rheology within the range needed for stable drop formation using the Ohnesorge equation [10]. The emission spectrum of a 0.01 wt% QD-silicone composite was measured and compared to the manufacturer's data for QDs (Fig. S1) [68]. The QD loading was selected as 0.005 wt% in Ink A (QD-Ink A) based on fluorescence detection limit experiments using fluorescence microscopy (Fig. S2) and the Einstein equation was used to predict the effect of QD loading on printability (Table 1) [69,70]. To enable composite curing, Ink B was prepared with added PtCl$_2$ with loadings of 0, 0.00075, 0.00125, 0.0025, and 0.005 wt% (Pt-Ink B). Inks were

Table 1

QD volume and mass, as determined from the manufacturer's specifications and crystallographic data for wurtzite CdSe and ZnS.

CdSe core diameter / nm	ZnS shell thickness / nm	Volume of a single QD / cm[3]	Estimated mass of a single QD / g
5.5	2.0	4.489×10^{-19}	1.946×10^{-18}

sonicated for 30 min prior to each use and cured in a 1:1 ratio of Ink A to Ink B.

2.3. Assessment of the effect of platinum loading on conversion and fluorescence

Raman spectroscopy was carried out with a Horiba LabRAM HR Raman microscope using a 785 nm laser (20 mW power), a 300 lines mm^{-1} grating and a 100x (0.75 NA) objective; the wavelength was selected to avoid QD fluorescence. Cured samples were prepared by mixing 175 μL of each ink and heating at 60 °C for 15 min. Ten Raman spectra were taken from the surface of each sample and averaged. The degree of conversion (DoC) was calculated using mean intensity ratios in comparison to cured SiliGlass. This microscope was also used with 532 nm excitation for XY fluorescence maps of samples containing quantum dots.

Well-plate reading was carried out using a Flexstation 3 multi-mode microplate reader (Molecular Devices). A Corning 4580 flat bottom half-area black well-plate was sequentially washed with acetone and iso-propyl alcohol before loading to remove any possible surface treatments. Curing was accelerated by heating with a heat gun for 15 min, followed by 2 h on a hotplate at 60 °C.

Fluorescence intensity counts were taken from the centre of each well, reading from the bottom. Measurements were taken between 25 and 40 °C at 2.5 °C intervals; 15–20 min were allowed between temperatures for samples to attain thermal equilibrium. Five measurements were then taken at 1.5 min intervals using 561 nm excitation wavelength and 630 nm emission wavelength for detection.

2.4. Luminescent temperature sensing

Confocal fluorescence microscopy was performed with a Zeiss LSM 710 microscope using a 20 × (0.50 NA) objective without immersion. 10 μL each of QD-Ink A (0.005 wt% QDs) and Pt-Ink B (0.00125 wt% PtCl$_2$) were deposited drop-on-drop on glass coverslips, heated at 60 °C for 15 min, and left overnight. Samples were excited at 561 nm using a DPSS laser with a 561 nm long-pass filter and lambda scans were taken from approximately 600 to 650 nm with 9.65 nm intervals (1024 ×1024 pixels, averaging of 4 frames); nominal wavelengths were 607 (602.55–612.20), 617 (612.20–621.85), 627 (621.85–631.50), 636 (631.50–641.15), and 646 (641.15–650.80) nm.

A prototype VAHEAT unit (Interherence) was used to ensure rapid and accurate temperature control. Lambda scans were taken between 25 and 60 °C at 2.5 °C intervals for three thermal cycles, allowing time for equilibration: 2 min for intervals of 2.5 °C and 15 min between thermal cycles. Scans were analysed using FIJI and ImageJ; while thermal drift was minimal, the Image Stabilizer plugin was used to align images. Background removal was carried out by applying a threshold to the 627 nm slice at 25 °C to obtain a background mask, which was applied consistently across all slices and stacks of the same thermal cycle. Greyscale data was then obtained from pixels and the mean greyscale values were used to assess emission intensity.

2.5. Inkjet printing

Printing trials were carried out using a Fujifilm Dimatix printer (DMP-2830) to confirm that composites for sensing could be deposited and cured with controlled patterning. QD-Ink A (0.005 wt%) and Pt-Ink B (0.00125 wt% PtCl$_2$) were printed using surface microstructuring to aid ink pinning: [59,71] a pinned grid consisting of one layer each of Ink A and Ink B was deposited and allowed to cure before depositing further material. QD-Ink A (0.005 wt% QDs) and Pt-Ink B (0.00125 wt% PtCl$_2$) were loaded into LCP cartridges and jetted at 30 V with 35 °C nozzle temperature and 60 °C substrate temperature to maximise cure rate. Surface microstructuring was used to overcome depinning on fluorosilanised glass slides [59,71]. Pinned grids were deposited by printing one layer of QD-Ink A followed by one layer of Pt-Ink B - or 1a1b - and were allowed to cure for 5 min. Subsequent material was then deposited to produce a film. Both grid and subsequent layers were deposited at 60 μm spacing to minimise realignment steps. Prints were imaged using a Nikon Eclipse LV100 ND optical microscope and analysed using ImageJ.

3. Results and discussion

3.1. Effect of the QD loading on ink viscosity

Ink A and Ink B addition cure inks were formulated from PolyTek SiliGlass, 50 wt% in octyl acetate solvent, similar to the reactive inks used by Sturgess et al. [59] Core shell CdSe/ZnS quantum dots with emission peak 630 nm were incorporated in Ink A with 0.005 wt% QD loading, henceforth referred to as QD-Ink A, based on fluorescence measurements (Fig. S2) and predicted viscosity (Table 1).

The effect of the QD loading on ink viscosity was estimated using the Einstein equation (Eq. 1): [69].

$$\mu_r = 1 + 2.5\phi \tag{1}$$

where μ$_r$ is relative viscosity and φ is the volume fraction of hard sphere particles. The estimated volume and mass of the supplied CdSe/ZnS QDs are shown in Table 1, as calculated using the density of wurtzite crystal structures.

Using the values above to calculate the QD volume fraction for 0.005 wt% QD-Ink A, the predicted relative viscosity for 0.005 wt% QDs in Ink A was found to be 1.00003 μ$_r$, meaning that the addition of 0.005 wt% QDs has no measurable effect on viscosity. Thus, the expected rheological parameters and printability of Ink A and Ink B are as shown in Table 2. The values for Ink A and 0.005 wt% QD-Ink A are expected to be identical to each other. Using the Ohnesorge equation to determine the printability parameter Z, it was found that both inks were within the range of stable droplet formation ($1 < Z < 10$) at 1.71 and 1.51, for Ink A and Ink B respectively [10].

Adequate silicone curing in the presence of QDs was not achieved for printing with 40–60 °C substrate heating. It has been reported that labile amine stabilising ligands can poison the platinum catalyst in QD silicone composites [63–65]. To overcome catalyst poisoning by the octadecylamine ligands, platinum (II) chloride was added to Ink B, henceforth referred to as Pt-Ink B. Loading was varied in order to test the effect of additional catalyst on curing and QD fluorescence.

Table 2

Printability of 50 wt% silicone inks in octyl acetate at 25 °C based on measured rheological parameters. Values of shear viscosity, density, surface tension, and the printability parameter Z are given for each ink.

	Viscosity η / mPa s	Density ρ / g cm^{-3}	Surface tension σ / mN m^{-1}	Diameter L / μm	Z
50 wt% SiliGlass A in octyl acetate (Ink A, crosslinker)	12.71 (±0.01)	0.92 (±0.01)	23.94 (±0.01)	21.5	1.71
50 wt% SiliGlass B in octyl acetate (Ink B, catalyst)	14.38 (±0.01)	0.95 (±0.01)	23.04 (±0.04)	21.5	1.51

3.2. Effect of platinum loading on conversion

Raman spectroscopy was used to compare the degree of conversion (DoC) in the cured inks by quantifying the unreacted silane moieties. Fig. 1 shows the Raman spectra of the cured inks normalised to the intensity of the Si-O-Si vibration at 490 cm^{-1}, and the inset shows the peak centred at 2150 cm^{-1} which corresponds to the Si-H stretching mode [72]. The Si-H peak intensity decreases as the reaction proceeds: the normalised intensity was 0.012 for the control inks (no QDs or additional catalyst) and 0.0066, 0.0065, and 0.0091 for the 0.00125, 0.0025, and 0.005 wt% Pt-Ink B with QD-Ink A, respectively. The control inks had the greatest residual silane, approximately twice that of moderate PtCl$_2$ loadings (0.00125 and 0.0025 wt%).

The intensity ratio between the Si-H (at 2150 cm^{-1}) and Si-O-Si peaks (at 490 cm^{-1}) was used to calculate the degree of conversion relative to cured SiliGlass, as described by Equation 2 (R = I$_{Si-H}$/I$_{Si-O-Si}$) [72,73]. Raman shifts, intensities, and the DoC for each sample is shown in Table. The relative DoC was 38 % for the control inks and 69 %, 70 %, and 49 % for 0.00125, 0.0025, and 0.005 wt% Pt-Ink B mixed with QD-Ink A, respectively. The addition of solvent increased the conversion relative to SiliGlass in all cases, despite increasing the cure time; the decrease in viscosity may benefit overall conversion by promoting mixing.

Additional platinum catalyst resulted in higher relative DoC than the control inks at all loadings, despite the presence of quantum dots. As the curing is diffusion rate-limited [74], higher catalyst concentration leads to faster and more homogenous cross-linking as the average distance between reaction centres is shortened. However, a 30 % decrease in DoC was observed between moderate and high PtCl$_2$ loading, suggesting that sufficiently high catalytic loading hinders conversion despite high initial cure rate.

$$DoC \quad (\%) = \left(1 - \frac{R_{sample}}{R_{control}}\right) * 100 \qquad (2)$$

3.3. Effect of platinum loading on fluorescence

Fluorescence maps of the cured QD-silicone samples were obtained in addition to Raman spectra to assess the effect of catalyst loading on emission, as shown in Fig. 2. Significant quenching was observed with additional catalyst: the average intensity at the fluorescence peak

maximum was 1650, 500, and 145 for 0.00125, 0.0025, and 0.005 wt% Pt-Ink B, respectively, which corresponds to a 70 % decrease in emission intensity as PtCl$_2$ concentration doubles. This suggests that the platinum may induce quenching.

It is well-known that metal ions can quench the fluorescence of quantum dots, as utilised for optical sensing. [75] One such mechanism is metal-induced agglomeration, which occurs where metals have high affinity for the QD stabilising ligands, stripping ligands from the quantum dot surface and leading to exposure of surface defects and to aggregation [76]. The fluorescence of CdSe-based QDs is enhanced by primary amines, for which the platinum catalyst has strong affinity, and such enhancement would also be removed upon loss of ligand [66,67]. A metal-induced agglomeration mechanism could rationalise the observed reductions in emission intensity and DoC: higher PtCl$_2$ concentration leads to high initial cure rate but induces greater aggregation, leading to greater liberation of ligands from joined QD surfaces which then poison the catalyst. Further spectroscopic analysis is needed to confirm the mechanism.

Well-plate reading was used to quantify the effect of additional platinum catalyst on the emission of cured QD-silicone composites and to identify the optimal loading for sensing. Emission intensity data for the cured QD-silicone composites (prepared from 0, 0.00075, 0.00125, 0.0025, and 0.005 wt% Pt-Ink B) is shown in Fig. 3; data collected during thermal cycles at each PtCl$_2$ loading is shown in Fig. 3(a-e) and Table S3. Increasing catalyst concentration was associated with a decrease in emission intensity from 1.0 to 0.11 AU for 0 and 0.005 wt% Pt-Ink B, respectively. However, a large difference in intensity was seen between low loadings (approximately 0.96 AU for 0.00075 and 0.00125 wt% Pt-Ink B) and high loadings (approximately 0.12 AU for 0.0025 and 0.005 wt% Pt-Ink B). This is in contrast with uncured inks, where emission intensity decreased at a relatively uniform rate with increasing catalyst concentration. This suggests a trade-off between Pt-induced quenching and the improved passivation arising from the accelerated curing of the matrix. Therefore, it is recommended that loading does not exceed 0.00125 wt% Pt-Ink B as quenching becomes significant and signal-to-noise ratio decreases.

A linear decrease in emission intensity with increasing temperature was seen in all well-plate reader samples for both thermal cycles of 30–40 °C (Fig. 3(a)-(e)), as expected of CdSe-based QDs immobilised in a polymer matrix [32,38,77]. Thermal coefficients were obtained from lines of best fit (summarised in Table S1); all samples with added
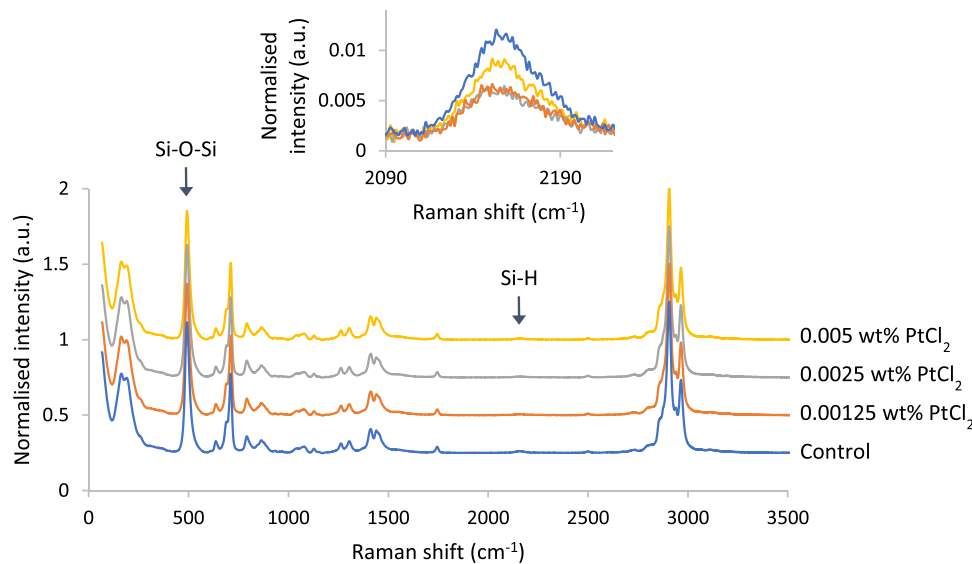
Fig. 1. Mean Raman spectra of the cured inks (N = 10); inset shows the Si-H stretching vibration at 2150 cm^{-1}. The blue line corresponds to the control sample, Ink A and Ink B. Other samples contain QD-Ink A and Pt-Ink B: orange, grey, and yellow lines show data for 0.00125 wt%, 0.0025 wt%, and 0.005 wt% Pt-Ink B. Spectra have been normalised to the intensity of the Si-O-Si mode at 490 cm^{-1} and offset on the y-axis for visual clarity.
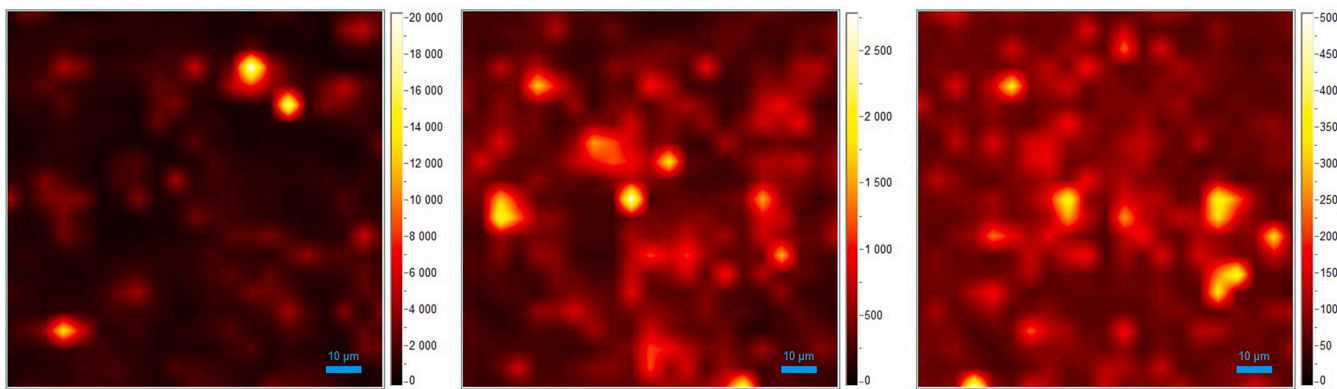
Fig. 2. Fluorescent maps of 0.005 wt% QD-silicone composites synthesised with additional platinum catalyst in Ink B. From left to right: samples made using (a) 0.00125, (b) 0.0025, and (c) 0.005 wt% Pt-Ink B. The intensity scale corresponds to the intensity of the emission maximum (in counts). Scale bar 10 μm.
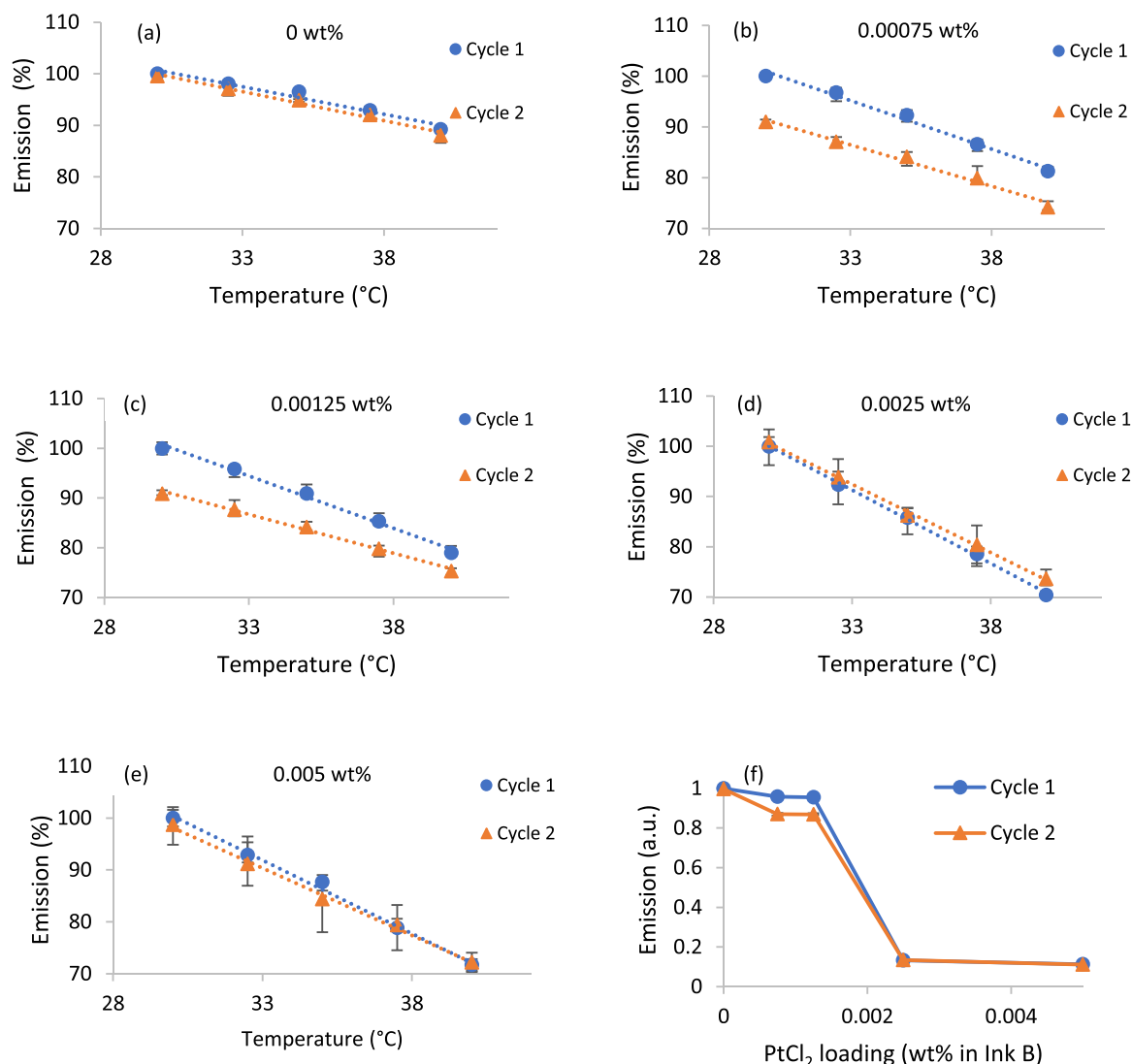
Fig. 3. Emission of cured QD-silicone composites. Bars display the range of values. Emission as a function of temperature for each loading of additional catalyst ((a)-(e)). Emission as a function of additional platinum catalyst at 30 °C (f).

catalyst showed decreased thermal sensitivity on the subsequent thermal cycle, where the magnitude of the decrease was greater in samples with greater emission intensity (Fig. 3(f)). Approximately 13.5 and 24.8 % decreases in thermal coefficient were observed between thermal cycles for 0.00075 and 0.00125 wt% $PtCl_2$, respectively.

Percentage emission intensity thermal coefficients increased with higher catalyst concentration and lower emission intensity, as platinum-induced quenching led to weaker signal strength. However, sensitivity

as a function of intensity count was highest for low $PtCl_2$ loadings (0.00075 and 0.00125 wt% $PtCl_2$ Ink B), followed by the sample without added catalyst. Therefore, although high loadings of catalyst led to higher apparent sensitivity, low loadings are recommended for higher signal-to-noise ratios and to minimise platinum-induced quenching.

3.4. Fluorescence temperature sensing

Based on the well-plate reading data, 0.00125 wt% $PtCl_2$ was selected as the loading for Pt-Ink B to maximise curing without compromising fluorescence. Confocal laser scanning microscopy (cLSM) was used to further assess the printable formulation via imaging to obtain data on QD aggregate size and dispersion in the silicone matrix and to characterise the thermal sensitivity of the material.

A micrograph of the QD-silicone sample prepared using 0.00125 wt % $PtCl_2$-Ink B is shown in Fig. S3. Clusters observed had approximately 4.5 µm mean Feret diameter, 3.9 µm modal, and 1.5–7.5 µm range. QD aggregates of varied size observed in the samples are similar to the unclonable patterns observed by Elliott et al. [70] Three thermal cycles of 25–60 °C were performed and lambda scans were taken at 2.5 °C intervals for 607–646 nm nominal emission wavelength. Intensity data was collected from greyscale values of individual pixels in images following background removal.

In quantum dots, emission intensity decreases with increasing temperature as a result of thermally-activated crossover [22,38]. The change in intensity of QDs is linear and reversible in the ambient temperature range (approximately 5–60 °C), resulting in a constant thermal sensitivity desirable for sensing. Fig. 4 shows the emission intensity (i.e. mean greyscale value) as a function of temperature, expressed as a percentage of the value for 627 nm emission at 30 °C. Emission intensity at wavelengths ≤ 627 nm decrease linearly between 30 and 60 °C, as expected [32,38,77]. Emission intensity at wavelengths above 627 nm show greater curvature: intensity initially increases with temperature as red-shift occurs but begins to decrease at higher temperatures as thermal quenching increases [38,39].

The temperature range investigated in this work is mainly suitable for bio-application. For applications where higher temperatures are required, it may be possible to use a similar approach with alternate QDs. Bulk QD-polymers have been observed to have linear emission up to 100 °C and reversible emission up to 150 °C [77], while Gu et al. achieved sensing on GaN LED chips with PbSe QDs sealed in silicone for a temperature range of 30–120 °C [34].

Percentage intensity thermal coefficients for three thermal cycles were obtained from lines of best fit (Table S2). The average percentage

intensity thermal coefficient obtained for the emission peak at 627 nm (-0.8 % °C^{-1}) is much greater than typical inkjet-printed sensors (0.1–0.3 % °C^{-1}) [11,12] and is within range of those reported for intensity-based sensing using CdSe/ZnS core-shell QDs, as shown in Table 3.

As emission intensity is dependent on concentration and laser power [22], the mean emission wavelength was estimated to assess red-shift for spectral shift-based sensing, as an alternate strategy which is independent of these factors. Quantum dots have characteristic spectral changes with temperature, namely emission peak red-shift and broadening [38,39]. The emission peak, λ_{max}, reflects the average QD bandgap size: bandgap shrinkage occurs as temperature increases, as described by the Varshni equation, leading to red-shift [78]. However, the complete origins of peak shift are complex as emission includes core and surface states, which may be accounted for by a semi-classical Marcus–Jortner electron transfer model [66].

The emission peak was estimated by finding the mean emission wavelength based on greyscale values, as the lambda scan collected a histogram of the emission spectra with 9.65 nm intervals (Fig. S4). The mean emission wavelength as a function of temperature was calculated according to Eq. S1 and is plotted in Fig. 5 and the estimated spectral shift thermal coefficients of thermal cycles are listed in Table 4. Average emission wavelength was seen to have a linear relationship with temperature, as is expected for CdSe/ZnS quantum dot fluorescence across a small, ambient temperature range [39,79].

The average spectral shift thermal coefficient for the three thermal cycles was 0.0677 nm °C^{-1}. Values for mean emission wavelength at specific temperatures were similar between cycles, in contrast to emission intensity, and show a clear, linear temperature dependence. This may suggest that spectral-based sensing would remain reliable across thermal cycles at these temperatures, although further studies of thermal cycles with higher spectral resolution are needed to confirm repeatability and investigate hysteresis (Table 5).

The estimated thermal coefficient of spectral shift is within the lower range of values reported for CdSe/ZnS QDs: 0.07–0.10 nm °C^{-1} [32,33, 39,79]. This suggests that the material has suitable fluorescence for spectral-based thermometry, and potentially may even be implemented where data collection has limited spectral resolution. The coefficient provides the primary information about the material however characterisation data under different conditions need to be considered for future device design, as implementation of sensing will introduce factors that alter how the sensor performs in practice. Method can introduce uncertainties as fluorescent parameters are compared to a reference image taken at room temperature, in addition to sensitivity to lighting
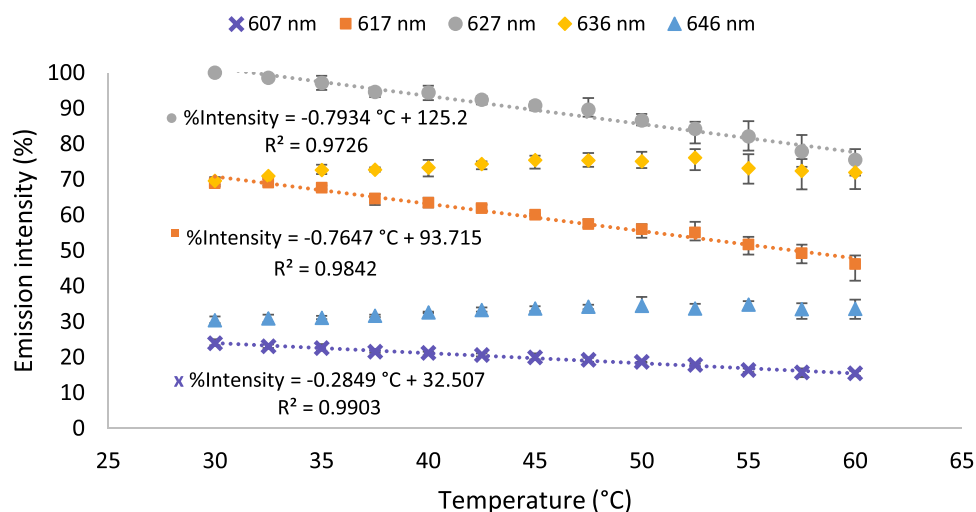
Fig. 4. Emission intensity of 0.00125 wt% $PtCl_2$ QD-silicone composite as a function of temperature at different emission wavelengths. Data shown is the average of the three thermal cycles; bars denote range of values.

Table 3

Raman shifts and intensities for Si-H and Si-O-Si modes obtained from cured samples and their relative DoC.

Sample	Si-H peak position cm^{-1}	Si-H peak intensity	Si-O-Si peak position cm^{-1}	Si-O-Si peak intensity	Intensity ratio R	Relative DoC %
SiliGlass A + SiliGlass B Undiluted	2157.1 (±3.4 SD)	18,904.6	491.9 (±0 SD)	643,342.0	0.029 (±0.001 SD)	''n/a''
Ink A + Ink B 50 wt% octyl acetate	2156.3 (±2.8 SD)	9185.1	491.9 (±0 SD)	50,3068.0	0.018 (±0.002 SD)	[38]
0.005 wt% QD-Ink A + 0.00125 wt% Pt-Ink B	2154.6 (±5.6 SD)	4815.0	492.2 (±0.7 SD)	520,240.2	0.009 (±0.001 SD)	[69]
0.005 wt% QD-Ink A + 0.0025 wt% Pt-Ink B	2152.7 (±7.4 SD)	4638.3	492.1 (±0.5 SD)	531,164.2	0.009 (±0.001 SD)	[70]
0.005 wt% QD-Ink A + 0.005 wt% Pt-Ink B	2154.5 (±4.9 SD)	7626.0	492.2 (±0.7 SD)	513,275.6	0.015 (±0.001 SD)	[49]
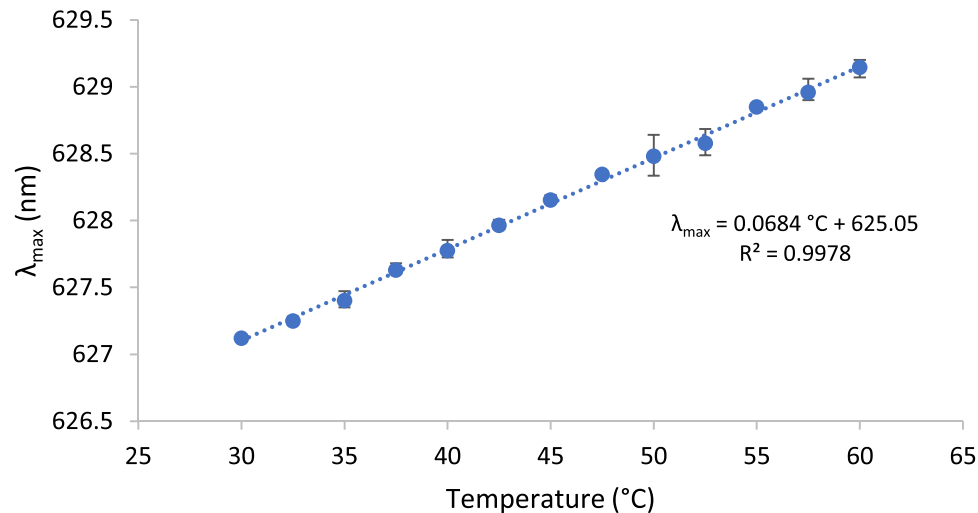
Fig. 5. Mean emission wavelength of 0.00125 wt% PtCl$_2$ QD-silicone composite as a function of temperature. Data shown is the average of the three thermal cycles; bars show the range of values obtained.

Table 4

Values reported for percentage intensity thermal coefficient for CdSe/ZnS quantum dots in literature. Papers where coefficients were not listed in text but could be obtained from the data presented are marked with an asterisk.

Thermal coefficient % °C^{-1}	Temperature range °C	QD emission wavelength nm	Dispersion medium	Author
-0.3	24.4–43.6	655	PDMS polymer used to fix position of individual QDs	Li et al. [33] *
-0.4 -0.7	20–70	655 620	Aqueous solution Unspecified polymer	Han et al. [30] *
-0.7 -1.6	10–50	600 520	Unspecified, non-hydrolytic sol gel	Jorge et al. [28]
-1.0 -1.3	-23–42 (250–315 K) 5–40 (278–313 K)	600	PLMA polymer	Walker et al. [38]
-1.3	30–60	640	PS polymer	Liu et al. [32]

Table 5

Estimated spectral shift thermal coefficients, calculated using mean emission wavelength from captured images of 0.00125 wt% PtCl$_2$ QD-silicone composite for each thermal cycle.

Thermal cycle					
1		2		3	
Thermal coefficient nm °C^{-1}	R^2 value	Thermal coefficient nm °C^{-1}	R^2 value	Thermal coefficient nm °C^{-1}	R^2 value
0.0677	0.9918	0.0671	0.9916	0.0702	0.9900

conditions. Moreover, further assessment and optimisation of composite photostability is needed to establish long-term performance but is beyond the scope of this paper.

3.5. Inkjet printing

As seen in the photograph of the circular test print (Fig. 6, Fig. S5), the composite inks successfully cured with controlled geometry and

visible fluorescence, demonstrating the first inkjet-printable QD-silicone composite. The surface texture was bumpy where ink conformed to the anchor points of the pinned grid; a more even surface texture may be achievable by depositing larger volumes of ink onto the pinned grid [59].

A pinned grid printed with 100 μm spacing (Fig. 6) highlights the accuracy of the surface microstructuring. The print pattern fits the pinned grid well, as shown by the overlay, and the final drop-on-drop Feret diameter is 37.5 μm ± 1.5 μm standard deviation. This is smaller than the smallest sessile drop diameters reported for silicone inkjet thus far: Sturgess et al. obtained 48 ± 2 μm drop diameters on a fluorosilanised glass substrate [59] and Mikkonen et al. achieved a drop diameter of 45 μm on spincoated-PDMS [62]. The uniform array and small drop-on-drop diameter suggest that comparatively high resolution is achievable.

Within individual drops, the quantum dots are not evenly distributed
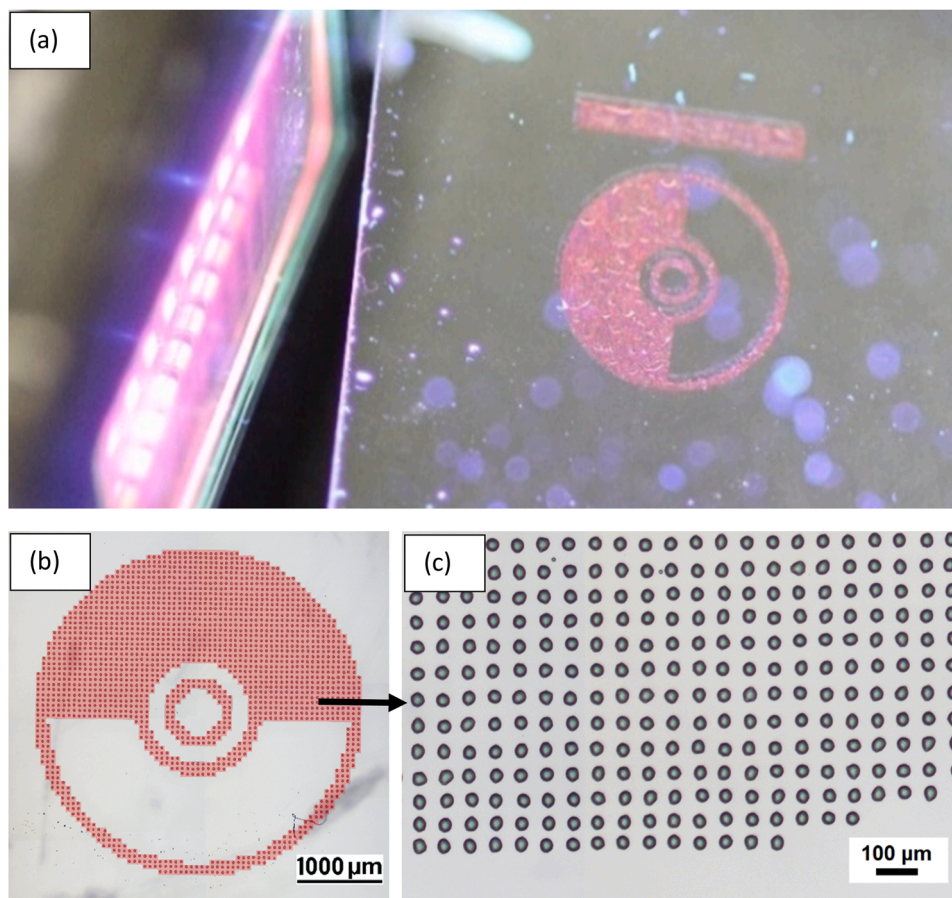
Fig. 6. (a) Photograph of the test print of 0.005 wt% QD-Ink A and 0.00125 wt% Pt Ink B, excited by a 395 nm UV lamp. The leader bar and print height is 7.9 cm. (b) Composite optical micrograph of a microstructuring grid deposited at 100 μm spacing, with print file overlay (red). (c) Close view of droplets array.

and form clusters of different sizes, as shown in Fig. S6. The pattern of clusters deposited appears to be random: Elliot et al. observed similar random patterns when jetting CdSe QDs in VeroClear (acrylate-based photopolymer) [70] and such unclonable patterns have applications in anti-counterfeiting [70,80]. Dispersion and stability of quantum dots in polymer matrices is challenging and there are a range of strategies to enhance QD compatibility with the host [48,81,82] and improve future ink formulations.

4. Conclusions

In summary, we report the first inkjet-printable bulk quantum dot-silicone nanocomposite for luminescence-based temperature sensing. Addition cure silicone inks containing CdSe/ZnS quantum dots were developed and a platinum catalyst (0.00125 wt% $PtCl_2$) was added to Ink B to overcome catalyst poisoning by QD ligands. Added catalyst enabled curing with almost double the degree of conversion compared to control inks, which contained neither QDs nor $PtCl_2$. However, as $PtCl_2$ loading was associated with decreased emission intensity, 0.00125 wt% $PtCl_2$ concentration was selected to ensure reliable printing with minimal loss of emission. Emission intensity of the printable composite showed a linear dependence on temperature from 30° to 60°C with a percentage intensity thermal coefficient of -0.68 to -0.93 % $°C^{-1}$ using confocal laser scanning microscopy; decrease in coefficient between thermal cycles suggests limited reusability. In contrast, estimations of spectral shift thermal coefficients were similar between sequential thermal cycles, which may indicate greater repeatability in addition to being independent of QD concentration and laser power. Further experiments and long-term photostability measurements are

required to assess and calibrate materials for use in demonstrative devices. Printing of films of QD-silicone nanocomposite with visible fluorescence was successfully demonstrated with 37.5 μm resolution. Overall, although further work is desirable to enhance photostability, this is a promising sensing material for the temperature range of 30–60 °C and its compatibility with inkjet printing can enable economical production of devices with minimally intrusive, in situ luminescence thermometry. We anticipate that this will be particularly beneficial for embedded sensing within microfluidic channels, especially where high spatial and thermal resolution are required.

CRediT authorship contribution statement

LB: Investigation, Formal analysis, Writing – original draft. **AF:** Conceptualization, Formal analysis, Writing – review & editing, Supervision. **GR:** Investigation, Formal analysis. **A. T:** Writing – review & editing. **RW:** Conceptualization, Writing – review & editing, Supervision. **CT:** Conceptualization, Writing – review & editing, Supervision.

Declaration of Competing Interest

The authors declare that they have no known competing financial interests or personal relationships that could have appeared to influence the work reported in this paper.

Data availability

Data will be made available on request.

Acknowledgements

Appendix A. Supporting information

Supplementary data associated with this article can be found in the online version at doi:10.1016/j.sna.2022.113977.

References

[1] M.J. Madou. Fundamentals of Microfabrication and Nanotechnology, Three-Volume Set, third ed., CRC Press, Boca Raton, 2018 https://doi.org/10.1201/9781315274164.

[2] D. Măriuța, S. Colin, C. Barrot-Lattes, S. Le Calvé, J.G. Korvink, L. Baldas, J. J. Brandner, Miniaturization of fluorescence sensing in optofluidic devices, Microfluid. Nanofluid. 24 (9) (2020) 65, https://doi.org/10.1007/s10404-020-02371-1.

[3] A. Moya, M. Ortega-Ribera, X. Guimerà, E. Sowade, M. Zea, X. Illa, E. Ramon, R. Villa, J. Gracia-Sancho, G. Gabriel, Online oxygen monitoring using integrated inkjet-printed sensors in a liver-on-a-chip system, Lab Chip 18 (14) (2018) 2023–2035, https://doi.org/10.1039/C8LC00456K.

[4] L. Nayak, S. Mohanty, S.K. Nayak, A. Ramadoss, A review on inkjet printing of nanoparticle inks for flexible electronics, J. Mater. Chem. C 7 (29) (2019) 8771–8795, https://doi.org/10.1039/C9TC01630A.

[5] S. Chung, K. Cho, T. Lee, Recent progress in inkjet-printed thin-film transistors, Adv. Sci. 6 (6) (2019), 1801445, https://doi.org/10.1002/advs.201801445.

[6] M. Hartwig, R. Zichner, Y. Joseph, Inkjet-printed wireless chemiresistive sensors—a review, Chemosensors 6 (4) (2018) 66, https://doi.org/10.3390/chemosensors6040066.

[7] S. Waheed, J.M. Cabot, N.P. Macdonald, T. Lewis, R.M. Guijt, B. Paull, M. C. Breadmore, 3D printed microfluidic devices: enablers and barriers, Lab Chip 16 (11) (2016) 1993–2013, https://doi.org/10.1039/C6LC00284F.

[8] I. Gibson, D. Rosen, B. Stucker, Additive Manufacturing Technologies, Springer, New York, NY, 2015, https://doi.org/10.1007/978-1-4939-2113-3.

[9] Y. Xu, X. Wu, X. Guo, B. Kong, M. Zhang, X. Qian, S. Mi, W. Sun, The boom in 3D-printed sensor technology, Sensors 17 (5) (2017) 1166, https://doi.org/10.3390/s17051166.

[10] B. Derby, Inkjet printing of functional and structural materials: fluid property requirements, feature stability, and resolution, Annu. Rev. Mater. Res. 40 (1) (2010) 395–414, https://doi.org/10.1146/annurev-matsci-070909-104502.

[11] B.A. Kuzubasoglu, S.K. Bahadir, Flexible temperature sensors: a review, Sens. Actuators A Phys. 315 (2020), 112282, https://doi.org/10.1016/j.sna.2020.112282.

[12] D. Barmpakos, G. Kaltsas, A review on humidity, temperature and strain printed sensors—current trends and future perspectives, Sensors 21 (3) (2021) 739, https://doi.org/10.3390/s21030739.

[13] Courbat, J.; Kim, Y.B.; Briand, D.; de Rooij, N.F. , Inkjet printing on paper for the realization of humidity and temperature sensors, in: Proceedings of the Sixteenth International Solid-State Sensors, Actuators and Microsystems Conference; IEEE, 2011, 1356–1359. https://doi.org/10.1109/TRANSDUCERS.2011.5969506.

[14] G. Mattana, T. Kinkeldei, D. Leuenberger, C. Ataman, J.J. Ruan, F. Molina-Lopez, A.V. Quintero, G. Nisato, G. Troster, D. Briand, N.F. de Rooij, Woven temperature and humidity sensors on flexible plastic substrates for E-textile applications, IEEE Sens. J. 13 (10) (2013) 3901–3909, https://doi.org/10.1109/JSEN.2013.2257167.

[15] M.D. Dankoco, G.Y. Tesfay, E. Benevent, M. Bendahan, Temperature sensor realized by inkjet printing process on flexible substrate, Mater. Sci. Eng. B 205 (2016) 1–5, https://doi.org/10.1016/j.mseb.2015.11.003.

[16] S. Ali, A. Hassan, J. Bae, C.H. Lee, J. Kim, All-printed differential temperature sensor for the compensation of bending effects, Langmuir 32 (44) (2016) 11432–11439, https://doi.org/10.1021/acs.langmuir.6b02885.

[17] C. Trudeau, P. Beaupré, M. Bolduc, S.G. Cloutier, All inkjet-printed perovskite-based bolometers, npj Flex. Electron. 4 (1) (2020) 34, https://doi.org/10.1038/s41528-020-00097-2.

[18] Lin, S.-C.; Liao, Y.-C. , Integrated humidity and temperature sensing circuit fabricated by inkjet printing technology, in: Proceedings of the Eleventh International Microsystems, Packaging, Assembly and Circuits Technology Conference (IMPACT), IEEE, 2016, 59–61. https://doi.org/10.1109/IMPACT.2016.7800045.

[19] Vena, A.; Sydanheimo, L.; Ukkonen, L.; Tentzeris, M.M. , A fully inkjet-printed chipless RFID gas and temperature sensor on paper, in: Proceedings of the IEEE RFID Technology and Applications Conference (RFID-TA), IEEE, 2014, 115–120. https://doi.org/10.1109/RFID-TA.2014.6934211.

[20] C. Bali, A. Brandlmaier, A. Ganster, O. Raab, J. Zapf, A. Hübler, Fully inkjet-printed flexible temperature sensors based on carbon and PEDOT:PSS1, Mater. Today Proc. 3 (3) (2016) 739–745, https://doi.org/10.1016/j.matpr.2016.02.005.

[21] T. Vuorinen, J. Niittynen, T. Kankkunen, T.M. Kraft, M. Mäntysalo, Inkjet-printed graphene/PEDOT:PSS temperature sensors on a skin-conformable polyurethane substrate, Sci. Rep. 6 (1) (2016) 35289, https://doi.org/10.1038/srep35289.

[22] D. Jaque, F. Vetrone, Luminescence nanothermometry, Nanoscale 4 (15) (2012) 4301–4326, https://doi.org/10.1039/c2nr30764b.

[23] M.D. Dramićanin, Trends in luminescence thermometry, J. Appl. Phys. 128 (4) (2020), 040902, https://doi.org/10.1063/5.0014825.

[24] F. Yang, N. Yang, X. Huo, S. Xu, Thermal sensing in fluid at the micro-nano-scales, Biomicrofluidics 12 (4) (2018), 041501, https://doi.org/10.1063/1.5037421.

[25] D. Choudhury, D. Jaque, A. Rodenas, W.T. Ramsay, L. Paterson, A.K. Kar, Quantum dot enabled thermal imaging of optofluidic devices, Lab Chip 12 (13) (2012) 2414–2420, https://doi.org/10.1039/c2lc40181a.

[26] P. Reiss, M. Protière, L. Li, Core/shell semiconductor nanocrystals, Small 5 (2) (2009) 154–168, https://doi.org/10.1002/smll.200800841.

[27] M. Chern, J.C. Kays, S. Bhuckory, A.M. Dennis, Sensing with photoluminescent semiconductor quantum dots, Methods Appl. Fluoresc. 7 (1) (2019), 012005, https://doi.org/10.1088/2050-6120/aaf6f8.

[28] P.A.S. Jorge, M. Mayeh, R. Benrashid, P. Caldas, J.L. Santos, F. Farahi, Quantum dots as self-referenced optical fibre temperature probes for luminescent chemical sensors, Meas. Sci. Technol. 17 (5) (2006) 1032–1038, https://doi.org/10.1088/0957-0233/17/5/S16.

[29] T. Munro, L. Liu, C. Glorieux, H. Ban, CdSe/ZnS quantum dot fluorescence spectra shape-based thermometry via neural network reconstruction, J. Appl. Phys. 119 (21) (2016), 214903, https://doi.org/10.1063/1.4953223.

[30] B. Han, W.L. Hanson, K. Bensalah, A. Tuncel, J.M. Stern, J.A. Cadeddu, Development of quantum dot-mediated fluorescence thermometry for thermal therapies, Ann. Biomed. Eng. 37 (6) (2009) 1230–1239, https://doi.org/10.1007/s10439-009-9681-6.

[31] W. Liu, Y. Zhang, H. Wu, Y. Feng, T. Zhang, W. Gao, H. Chu, J. Yin, T. Cui, Y. Wang, J. Zhao, W.W. Yu, Planar temperature sensing using heavy-metal-free quantum dots with micrometer resolution, Nanotechnology 25 (28) (2014), 285501, https://doi.org/10.1088/0957-4484/25/28/285501.

[32] L. Liu, K. Zhong, L. Meng, D. Van Hemelrijck, L. Wang, C. Glorieux, Temperature-sensitive photoluminescent CdSe-ZnS polymer composite film for lock-in photothermal characterization, J. Appl. Phys. 119 (22) (2016), 224902, https://doi.org/10.1063/1.4953591.

[33] S. Li, K. Zhang, J.-M. Yang, L. Lin, H. Yang, Single quantum dots as local temperature markers, Nano Lett. 7 (10) (2007) 3102–3105, https://doi.org/10.1021/nl071606p.

[34] P. Gu, Y. Zhang, Y. Feng, T. Zhang, H. Chu, T. Cui, Y. Wang, J. Zhao, W.W. Yu, Real-time and on-chip surface temperature sensing of GaN LED chips using PbSe quantum dots, Nanoscale 5 (21) (2013) 10481–10486, https://doi.org/10.1039/c3nr02438e.

[35] L.M. Maestro, E.M. Rodríguez, F.S. Rodríguez, M.C.I. la Cruz, A. Juarranz, R. Naccache, F. Vetrone, D. Jaque, J.A. Capobianco, J.G. Sole, CdSe quantum dots for two-photon fluorescence thermal imaging, Nano Lett. 10 (12) (2010) 5109–5115, https://doi.org/10.1021/nl1036098.

[36] L.M. Maestro, Q. Zhang, X. Li, D. Jaque, M. Gu, Quantum-dot based nanothermometry in optical plasmonic recording media, Appl. Phys. Lett. 105 (18) (2014), 181110, https://doi.org/10.1063/1.4901258.

[37] P. Haro-González, L. Martínez-Maestro, I.R. Martín, J. García-Solé, D. Jaque, High-sensitivity fluorescence lifetime thermal sensing based on CdTe quantum dots, Small 8 (17) (2012) 2652–2658, https://doi.org/10.1002/smll.201102736.

[38] G.W. Walker, V.C. Sundar, C.M. Rudzinski, A.W. Wun, M.G. Bawendi, D.G. Nocera, Quantum-dot optical temperature probes, Appl. Phys. Lett. 83 (17) (2003) 3555–3557, https://doi.org/10.1063/1.1620686.

[39] D. Valerini, A. Cretí, M. Lomascolo, L. Manna, R. Cingolani, M. Anni, Temperature dependence of the photoluminescence properties of colloidal CdSe/ZnS core/shell quantum dots embedded in a polystyrene matrix, Phys. Rev. B 71 (23) (2005), 235409, https://doi.org/10.1103/PhysRevB.71.235409.

[40] L.M. Maestro, C. Jacinto, U.R. Silva, F. Vetrone, J.A. Capobianco, D. Jaque, J. G. Solé, CdTe quantum dots as nanothermometers: towards highly sensitive thermal imaging, Small 7 (13) (2011) 1774–1778, https://doi.org/10.1002/smll.201002377.

[41] H.M. Haverinen, R.A. Myllyla̧, G.E. Jabbour, Inkjet printing of light emitting quantum dots, Appl. Phys. Lett. 94 (7) (2009), 073108, https://doi.org/10.1063/1.3085771.

[42] C. Jiang, Z. Zhong, B. Liu, Z. He, J. Zou, L. Wang, J. Wang, J. Peng, Y. Cao, Coffee-ring-free quantum dot thin film using inkjet printing from a mixed-solvent system on modified ZnO transport layer for light-emitting devices, ACS Appl. Mater. Interfaces 8 (39) (2016) 26162–26168, https://doi.org/10.1021/acsami.6b08679.

[43] Y. Liu, F. Li, Z. Xu, C. Zheng, T. Guo, X. Xie, L. Qian, D. Fu, X. Yan, Efficient all-solution processed quantum dot light emitting diodes based on inkjet printing technique, ACS Appl. Mater. Interfaces 9 (30) (2017) 25506–25512, https://doi.org/10.1021/acsami.7b05381.

[44] P. Yang, L. Zhang, D.J. Kang, R. Strahl, T. Kraus, High-resolution inkjet printing of quantum dot light-emitting microdiode arrays, Adv. Opt. Mater. 8 (1) (2020), 1901425, https://doi.org/10.1002/adom.201901429.

[45] J. Lee, V.C. Sundar, J.R. Heine, M.G. Bawendi, K.F. Jensen, Full color emission from II-VI semiconductor quantum dot-polymer composites, Adv. Mater. 12 (15) (2000) 1102–1105, https://doi.org/10.1002/1521-4095(200008)12:15<1102::AID-ADMA1102>3.0.CO;2-J.

[46] M. Böberl, M.V. Kovalenko, S. Gamerith, E.J.W. List, W. Heiss, Inkjet-printed nanocrystal photodetectors operating up to 3 Mm wavelengths, Adv. Mater. 19 (21) (2007) 3574–3578, https://doi.org/10.1002/adma.200700111.

[47] H.-H. Moretto, M. Schulze, G. Wagner, Silicones. in: Ullmann's Encyclopedia of Industrial Chemistry, Wiley-VCH Verlag GmbH & Co. KGaA, Weinheim, Germany, 2000, pp. 675–708, https://doi.org/10.1002/14356007.a24_057.

[48] H. Moon, C. Lee, W. Lee, J. Kim, H. Chae, Stability of quantum dots, quantum dot films, and quantum dot light-emitting diodes for display applications, Adv. Mater. 31 (34) (2019), 1804294, https://doi.org/10.1002/adma.201804294.

[49] H.-S. Chen, C.-K. Hsu, H.-Y. Hong, InGaN-CdSe-ZnSe quantum dots white LEDs, IEEE Photonics Technol. Lett. 18 (1) (2006) 193–195, https://doi.org/10.1109/LPT.2005.859540.

[50] E. Jang, S. Jun, H. Jang, J. Lim, B. Kim, Y. Kim, White-light-emitting diodes with quantum dot color converters for display backlights, Adv. Mater. 22 (28) (2010) 3076–3080, https://doi.org/10.1002/adma.201000525.

[51] R. Hirayama, M. Naruse, H. Nakayama, N. Tate, A. Shiraki, T. Kakue, T. Shimobaba, M. Ohtsu, T. Ito, Design, implementation and characterization of a quantum-dot-based volumetric display, Sci. Rep. 5 (2015) 8472, https://doi.org/10.1038/srep08472.

[52] L. Kong, L. Zhang, Z. Meng, C. Xu, N. Lin, X.-Y. Liu, Ultrastable, highly luminescent quantum dot composites based on advanced surface manipulation strategy for flexible lighting-emitting, Nanotechnology 29 (31) (2018), 315203, https://doi.org/10.1088/1361-6528/aac39c.

[53] J.-S. Li, Y. Tang, Z.-T. Li, L.-S. Rao, X.-R. Ding, B.-H. Yu, High efficiency solid–liquid hybrid-state quantum dot light-emitting diodes, Photonics Res. 6 (12) (2018) 1107, https://doi.org/10.1364/PRJ.6.001107.

[54] H. Osman, W. Li, X. Zhang, F. Chun, W. Deng, M. Moatasim, X. Zheng, W. Deng, H. Zhang, W. Yang, One-step hot injection synthesis of gradient alloy CdxZn1-XSySe1-y quantum dots with large-span self-regulating ability, J. Lumin. 206 (2019) 565–570, https://doi.org/10.1016/j.jlumin.2018.10.089.

[55] I.D. Johnston, D.K. McCluskey, C.K.L. Tan, M.C. Tracey, Mechanical characterization of bulk sylgard 184 for microfluidics and microengineering, J. Micromech. Microeng. 24 (3) (2014), 035017, https://doi.org/10.1088/0960-1317/24/3/035017.

[56] D. Wang, J. Klein, E. Mejía, Catalytic systems for the cross-linking of organosilicon polymers, Chem. Asian J. 12 (11) (2017) 1180–1197, https://doi.org/10.1002/asia.201700304.

[57] P. Mazurek, S. Vudayagiri, A.L. Skov, How to tailor flexible silicone elastomers with mechanical integrity: a tutorial review, Chem. Soc. Rev. 48 (6) (2019) 1448–1464, https://doi.org/10.1039/C8CS00963E.

[58] Y. Peng, S. Xiao, J. Yang, J. Lin, W. Yuan, W. Gu, X. Wu, Z. Cui, The elastic microstructures of inkjet printed polydimethylsiloxane as the patterned dielectric layer for pressure sensors, Appl. Phys. Lett. 110 (26) (2017), 261904, https://doi.org/10.1063/1.4990528.

[59] C. Sturgess, C.J. Tuck, I.A. Ashcroft, R.D. Wildman, 3D reactive inkjet printing of polydimethylsiloxane, J. Mater. Chem. C 5 (37) (2017) 9733–9743, https://doi.org/10.1039/C7TC02412F.

[60] A. Mamidanna, C. Lefky, O. Hildreth, Drop-on-demand printed microfluidics device with sensing electrodes using silver and PDMS reactive inks, Microfluid. Nanofluid. 21 (11) (2017) 172, https://doi.org/10.1007/s10404-017-2010-8.

[61] D. McCoul, S. Rosset, S. Schlatter, H. Shea, Inkjet 3D printing of UV and thermal cure silicone elastomers for dielectric elastomer actuators, Smart Mater. Struct. 26 (12) (2017), 125022, https://doi.org/10.1088/1361-665X/aa9695.

[62] R. Mikkonen, P. Puistola, I. Jönkkäri, M. Mäntysalo, Inkjet printable polydimethylsiloxane for all-inkjet-printed multilayered soft electrical applications, ACS Appl. Mater. Interfaces 12 (10) (2020) 11990–11997, https://doi.org/10.1021/acsami.9b19632.

[63] J. Ziegler, S. Xu, E. Kucur, F. Meister, M. Batentschuk, F. Gindele, T. Nann, Silica-coated InP/ZnS nanocrystals as converter material in white LEDs, Adv. Mater. 20 (21) (2008) 4068–4073, https://doi.org/10.1002/adma.200800724.

[64] J. Weaver, R. Zakeri, S. Aouadi, P. Kohli, Synthesis and characterization of quantum dot–polymer composites, J. Mater. Chem. 19 (20) (2009) 3198–3206, https://doi.org/10.1039/b820204d.

[65] N.N. Trung, Q.-P. Luu, B.T. Son, L.H. Sinh, J.-Y. Bae, Preparation and characterization of silicone resin nanocomposite containing CdSe/ZnS quantum dots, Polym. Compos. 33 (10) (2012) 1785–1791, https://doi.org/10.1002/pc.22320.

[66] M.M. Krause, P. Kambhampati, Linking surface chemistry to optical properties of semiconductor nanocrystals, Phys. Chem. Chem. Phys. 17 (29) (2015) 18882–18894, https://doi.org/10.1039/C5CP02173A.

[67] D.P. Morgan, D.F. Kelley, Mechanism of hole trap passivation in cdse quantum dots by alkylamines, J. Phys. Chem. C 122 (44) (2018) 25661–25667, https://doi.org/10.1021/acs.jpcc.8b08798.

[68] Specification Sheet - QSP 630, Ocean Nanotech LLC, 2016.

[69] S.D. Hoath, Fundamentals of Inkjet Printing: the Science of Inkjet and Droplets, John Wiley & Sons, 2016, https://doi.org/10.1002/9783527684724.

[70] A.M. Elliott, O.S. Ivanova, C.B. Williams, T.A. Campbell, Inkjet printing of quantum dots in photopolymer for use in additive manufacturing of nanocomposites, Adv. Eng. Mater. 15 (10) (2013) 903–907, https://doi.org/10.1002/adem.201300020.

[71] S. Vafaei, C. Tuck, I. Ashcroft, R. Wildman, Surface microstructuring to modify wettability for 3D printing of nano-filled inks, Chem. Eng. Res. Des. 109 (2016) 414–420, https://doi.org/10.1016/j.cherd.2016.02.004.

[72] D. Cai, A. Neyer, R. Kuckuk, H.M. Heise, mid-infrared, near-infrared and ultraviolet–visible spectroscopy of PDMS silicone rubber for characterization of polymer optical waveguide materials, J. Mol. Struct. 976 (1–3) (2010) 274–281, https://doi.org/10.1016/j.molstruc.2010.03.054.

[73] E. Lempel, Z. Czibulya, S. Kunsági-Máté, J. Szalma, B. Sümegi, K. Böddi, Quantification of conversion degree and monomer elution from dental composite using HPLC and micro-Raman spectroscopy, Chromatographia 77 (17–18) (2014) 1137–1144, https://doi.org/10.1007/s10337-014-2647-3.

[74] J.R. Castrejón-Pita, K.J. Kubiak, A.A. Castrejón-Pita, M.C.T. Wilson, I. M. Hutchings, Mixing and internal dynamics of droplets impacting and coalescing on a solid surface, Phys. Rev. E 88 (2) (2013), 023023, https://doi.org/10.1103/PhysRevE.88.023023.

[75] P. Wu, T. Zhao, S. Wang, X. Hou, Semicondutor quantum dots-based metal ion probes, Nanoscale 6 (1) (2014) 43–64, https://doi.org/10.1039/C3NR04628A.

[76] J. Ke, X. Li, Q. Zhao, Y. Hou, J. Chen, Ultrasensitive quantum dot fluorescence quenching assay for selective detection of mercury ions in drinking water, Sci. Rep. 4 (1) (2015) 5624, https://doi.org/10.1038/srep05624.

[77] Y. Zhao, C. Riemersma, F. Pietra, R. Koole, C. de Mello Donegá, A. Meijerink, High-temperature luminescence quenching of colloidal quantum dots, ACS Nano 6 (10) (2012) 9058–9067, https://doi.org/10.1021/nn303217q.

[78] S. Chattopadhyay, P. Sen, J. Thomas Andrews, P. Kumar Sen, Semiconductor core-shell quantum dot: a low temperature nano-sensor material, J. Appl. Phys. 111 (3) (2012), 034310, https://doi.org/10.1063/1.3681309.

[79] A. Joshi, K.Y. Narsingi, M.O. Manasreh, E.A. Davis, B.D. Weaver, Temperature dependence of the band gap of colloidal CdSe/ZnS core/shell nanocrystals embedded into an ultraviolet curable resin, Appl. Phys. Lett. 89 (13) (2006), 131907, https://doi.org/10.1063/1.2357856.

[80] Y. Liu, F. Han, F. Li, Y. Zhao, M. Chen, Z. Xu, X. Zheng, H. Hu, J. Yao, T. Guo, W. Lin, Y. Zheng, B. You, P. Liu, Y. Li, L. Qian, Inkjet-printed unclonable quantum dot fluorescent anti-counterfeiting labels with artificial intelligence authentication, Nat. Commun. 10 (1) (2019) 2409, https://doi.org/10.1038/s41467-019-10406-7.

[81] N. Tomczak, D. Jańczewski, M. Han, G.J. Vancso, Designer polymer–quantum dot architectures, Prog. Polym. Sci. 34 (5) (2009) 393–430, https://doi.org/10.1016/j.progpolymsci.2008.11.004.

[82] P. Tao, Y. Li, R.W. Siegel, L.S. Schadler, Transparent luminescent silicone nanocomposites filled with bimodal PDMS-brush-grafted CdSe quantum dots, J. Mater. Chem. C 1 (1) (2013) 86–94, https://doi.org/10.1039/C2TC00057A.